Latin American Journal of Aquatic Research, 54(2): 289-309, 2026
DOI: 10.3856/vol54-issue2-fulltext-3531

Research Article

Seasonal wave, current, and suspended sediment dynamics on two contrasting microtidal beaches in the Colombian Caribbean

Julie K. Ruiz-Merchán [1,2,3,4], Juan C. Restrepo[1], Brian K. Haus[2,3], Luis Otero[1] Mario Conde-Frías[1], Jairo Cueto[7,8], Margarita Guerrero[5] Sindy Henriquez[1], José M. Rebellón[6] & Anlly Guerrero[1]

[1]Geosciences Research Group-GEO4, Department of Physics and Geosciences
Universidad del Norte, Barranquilla, Colombia
[2]The Alfred C. Glassell Jr. SUSTAIN Laboratory, Rosenstiel School of Marine
Atmospheric and Earth Science, University of Miami, Rickenbacker Causeway, Miami, USA
[3]Department of Ocean Sciences, Rosenstiel School of Marine
Atmospheric, and Earth Science, University of Miami, Rickenbacker Causeway, Miami, USA
[4]The Reef Institute, West Palm Beach, USA
[5] Faculty of Science, Education, Arts, and Humanities
Institución Universitaria de Barranquilla Barranquilla, Colombia
[6]College of Engineering and Computer Science, University of Central Florida, Orlando, FL, USA
[7]Department of Natural and Exact Sciences Research Group in Natural and Exact Sciences-GICNEX
Universidad de la Costa, Barranquilla, Colombia
[8]Coastal Geology and Sedimentology Group, Institute of Geosciences, Kiel University, Germany
Corresponding author: Julie K. Ruiz-Merchán (merchanj@uninorte.edu.co)

ABSTRACT. Waves are the primary phenomenon to be considered in coastal engineering studies and designs, as they constitute the primary source of energy driving coastal flows and processes. This study examines the roles of gravity (G) and infragravity (IG) waves in suspended sediment transport within the surf zones of two Caribbean beaches in Colombia: the reflective-intermediate beach, Costa Verde, and the dissipative-intermediate beach, Bocagrande. Field measurements included free-surface elevation (η), cross-shore (u) and alongshore (v) velocities, and sediment corrected backscatter (SCB, in dB). Results indicate higher sediment suspension during the dry season, with IG wave energy dominating cross-shore and alongshore currents. Strong correlations between u and v components and SCB, revealed by Cross Wavelet Transform (XWT) and Wavelet Transforms Coherence (WTC), show that IG waves largely control sediment flux. Energy and SCB fluxes did not exhibit a uniform direction, reflecting complex interactions with beach morphology, wave breaking, and anthropogenic structures. Overall, IG-driven currents are the primary factor controlling suspended-sediment transport and morphodynamic evolution in the surf zone. These findings provide essential insights for coastal management and the planning of erosion-mitigation measures for urban beaches.

Keywords: hydrodynamic; infragravity wave; gravity wave; sediment transport; cross-shore and alongshore currents

INTRODUCTION

In microtidal beach environments, suspended sediment transport plays a fundamental role in shaping coastal morphology, especially in the surf zone, where wave breaking generates energy that mobilizes sediment (Aagaard & Greenwood 2008). Superficial sediment suspension -that is, the transport of particles near the water surface- is mainly driven by wave breaking, the undertow current, and the orbital motions of waves (Hsu & Hanes 2004, Aagaard & Greenwood 2008).

Associate Editor: Marcela Cornejo

In the marine environment, gravity (G) waves with periods ranging from 1 to 30 s are generated by wind and propagate along the sea surface. Infragravity (IG) waves, by contrast, have longer periods (30-300 s, occasionally up to 500 s), originate within the water column -particularly in coastal zones-and are associated with wave groupiness. Both wave types play a critical role in suspension dynamics. G waves, characterized by shorter periods, directly generate drag and lifting forces near the seabed. IG waves, arising from the interaction and modulation of wind waves, induce fluctuations in water depth and horizontal accelerations that enhance sediment suspension and near-surface transport (Guza & Thornton 1982, Feddersen et al. 2000). Within the surf zone, sediment is resuspended from the seabed and transported by surface currents or vortex bores in cross-shore and alongshore directions (Elgar et al. 2001, Scott et al. 2011). In microtidal environments (tidal range <2 m), wave energy is the dominant driver of sediment transport and morphological variability, surpassing tidal forcing (Short & Neckles 1999).

Wave height and period, breaker type, grain size, and seabed slope strongly influence the spatial and temporal patterns of superficially suspended sediment in the surf zone (O'Donoghue & Wright 2004). Under high-energy conditions, the upward sediment flux can increase significantly, leading to elevated concentrations of suspended material even in the upper water column (Austin & Masselink 2006). This sediment is then redistributed along the profile, contributing to bar migration and berm erosion or accretion, depending on wave energy and the net direction of sediment transport (Baldock et al. 2004, Auer et al. 2025). Understanding surface-layer transport mechanisms is crucial for accurately predicting short-term beach responses to extreme events, especially on microtidal coasts that are highly sensitive to wave dynamics.

Two main generation mechanisms have been proposed for IG waves. The first, known as Bound Long Waves (Longuet-Higgins & Stewart 1962, 1964), indicating that IG waves are produced by non-linear interactions between G waves outside the breaking zone. The second mechanism, referred to as the Time Varying Breakpoint, was described by Symonds et al. (1982) based on a low-frequency wave generation model over a variable seabed. In this case, breaking point movement is regarded as the generating mechanism. Both mechanisms are complementary and may coexist, establishing a complex flow in which it is hard to differentiate between them (Schaffer 1994).

IG waves can be classified as bound long waves, leaky waves, and edge waves. Before breaking, low-frequency oscillations often take the form of bound (or forced) long waves. These waves do not exist on their own; they are generated and maintained by another wave process. After breaking, they can persist as free waves, as the bound long wave is released. Free waves may be leaky waves, reflected towards the sea after breaking. Free waves may also be edge waves that remain trapped nearshore by refraction, thus contributing to rhythmic coastal features such as beach cusps (Longuet-Higgins & Stewart 1962). Leaky and edge waves may occur either as progressive or standing, and their direction may be cross-shore as well as alongshore (Péquignet et al. 2009).

Several recent studies have emphasized the complexity of IG wave dynamics and their influence on sediment transport and coastal morphology. Winter et al. (2017) demonstrated that in coastal zones with irregular bathymetry, artificial structures such as groins and rocky outcrops can induce standing IG waves through partial wave reflection, thereby intensifying nearshore sediment suspension. Montaño-Muñoz et al. (2018) further supported this by identifying standing-edge waves trapped by coastal features, which significantly affect sediment fluxes and beach morphology. Additionally, Bowen & Huntley (1984) highlighted the importance of currents associated with the IG regime as a dominant mechanism in sediment advection, shaping morphodynamic responses in surf zones. This body of work underscores the need to consider both natural and anthropogenic influences on wave dynamics to understand sediment transport processes in microtidal beach environments fully.

Some studies have contributed to the classification of nearshore IG waves by analyzing phase relationships between variables such as the evolution of free-surface elevation (η), u, and v (Holman 1981, Péquignet et al. 2009). In edge and leaky waves with cross-shore and standing longshore directions, respectively, the difference between u and v relative to η is 90°, whereas the difference between u and v ranges from 0 to 180° (Huntley & Bowen 1973, Guza & Thornton 1982). On the other hand, for progressive leaky waves, in either the cross-shore or alongshore direction, the velocity components (u, v) are in phase with η at 0°. In contrast, the phase angle between u and v may be either 0 or 180° (Huntley & Bowen 1973, Goodfellow & Stephenson 2008).

Ruiz-Merchán et al. (2019) previously assessed hydrodynamics at Costa Verde beach, the area considered here. It was characterized as a reflective-

intermediate beach through the Cross Wavelet Transform (XWT) and Wavelet Coherence Transform (WTC) analyses during two climate seasons. In the dry season, leaky IG waves were identified in the cross-shore and standing alongshore directions, together with cross-shore and standing alongshore edge waves. During the wet season, specifically in the area farthest from the shore, leaky waves were identified propagating cross-shore and progressively alongshore. At the same time, the prevailing waves closer to the shore were cross-shore and standing alongshore leaky waves, mostly propagating alongshore due to reflection dynamics. Ruiz-Merchán et al. (2025) studied hydrodynamics at Bocagrande Beach using XWT and WTC analyses. The authors reported the presence of cross-shore and standing alongshore leaky waves during the dry season, both in the closest and farthest portions of the coast. In the area closest to the coast, cross-shore and standing alongshore edge waves were observed, given that the beach is located between two groins. During the wet season, cross-shore and progressive alongshore leaky waves prevailed close to the coast.

In Cueto & Otero (2020), the morphodynamic response to extreme swell events generated by hurricanes and cold fronts was assessed for microtidal beaches, both dissipative and reflective, in the Colombian Caribbean. Regardless of beach configuration (dissipative -intermediate or reflective-intermediate), erosive processes were more pronounced during cold fronts (March 2009 and December 2017) than under hurricane conditions. This behavior may be related to factors such as wave direction, wave period, or event duration. Bocagrande Beach is more exposed to extreme wave events, mostly due to its characteristic dissipative profile. IG energy, essential to sediment transport dynamics, does not reflect off the beachfront but instead dissipates within the flooded area, dragging sediment into the sea. In contrast, Costa Verde, due to its beach profile, exhibits conservative shoreline retreats.

Conceptual models of beach states were first developed by Wright & Short (1984). Subsequent studies have analyzed G and IG waves in different coastal environments (Montaño-Muñoz et al. 2018, Ruiz-Merchán et al. 2019, 2025, Cueto & Otero 2020). However, a gap remains in understanding how these waves regulate hydrodynamic processes and, consequently, the dynamics of sediment transport on beaches exposed to both natural and anthropogenic pressures. This limitation reduces the ability to anticipate the morphodynamic evolution of beaches and hinders the design of effective coastal management strategies. In urban settings such as Bocagrande and Costa Verde, where erosion, sand loss, and infrastructure vulnerability are recurrent problems, understanding the interactions among G and IG waves and hydrodynamic forcings is essential for improving planning and decision-making for coastal protection, restoration, and sustainable use.

This study builds on previous works (Ruiz-Merchán et al. 2019, 2025) and advances this line of research by addressing unresolved questions, particularly the relationship between sediment-corrected backscatter (SCB, dB) and the distribution of G and IG wave energy in the surf zone. The specific objective is to evaluate how G and IG waves influence the hydrodynamic forcings that modulate sediment transport at Costa Verde, a reflective-intermediate beach, and Bocagrande, a dissipative -intermediate beach- both microtidal systems with contrasting morphodynamic characteristics. The broader aim of the study is to generate knowledge applicable to coastal management, particularly for erosion mitigation and the planning of conservation and recreational strategies.

MATERIALS AND METHODS

This section presents the methods used to analyze sediment transport in the surf zone. Building on previous studies (Aagaard & Greenwood 2008, Ruiz-Merchán et al. 2019, 2025), the relationship between sediment-corrected backscatter (SCB, in dB), G, and IG wave energy was analyzed.

Study area

The study area is located in the Colombian Caribbean, specifically at Bocagrande Beach in Cartagena and at Costa Verde Beach in the municipality of Ciénaga (Fig. 1). The tidal regime along the Colombian Caribbean coast varies, with an average amplitude of 20-30 cm and occasional values exceeding 50 cm. Therefore, it is classified as a diurnal mixed microtidal zone (Wiedemann 1973, Kjerfve 1981, Garcia et al. 2011, Restrepo et al. 2012, Andrade et al. 2013).

Both study areas are beaches that are affected by adjacent artificial structures and natural sediment sources. Bocagrande Beach lies between two groins that influence local hydrodynamics, thereby promoting erosion. In addition to two adjacent groins, Costa Verde is influenced by the mouth of the Cordoba River (Fig. 2a), located 1 km from the beach, which affects hydrodynamics and sediment transport. According to Ruiz-Merchán et al. (2019, 2025), Bocagrande is classified as a microtidal dissipative-intermediate beach,

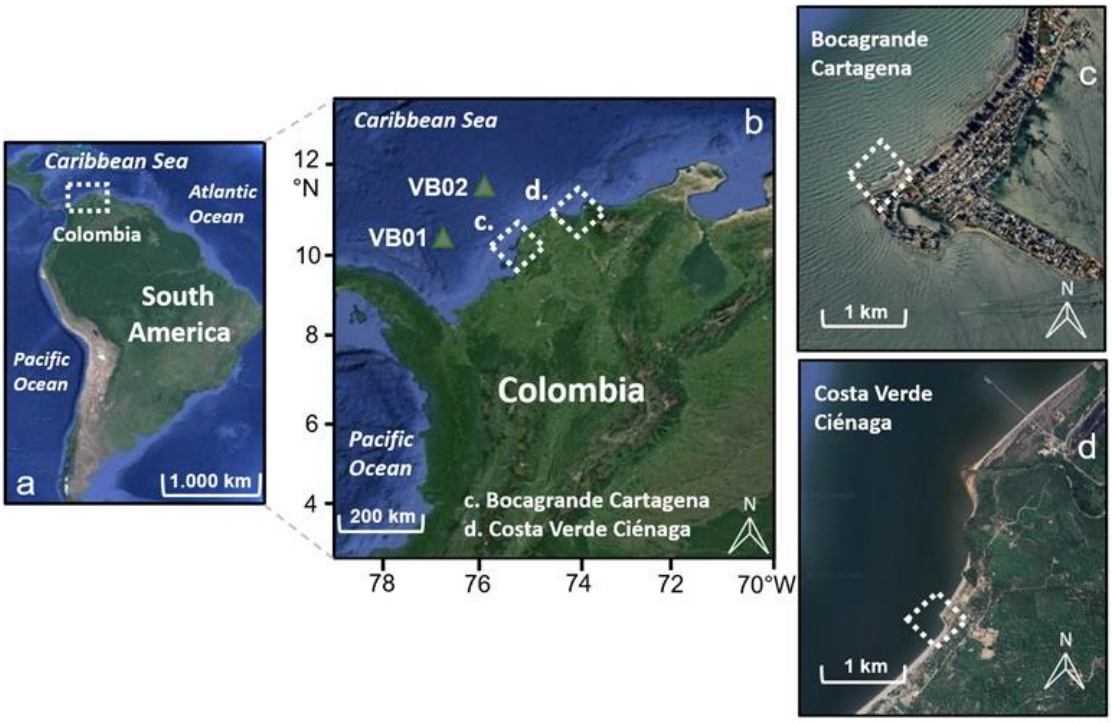

Figure 1. a) Geographical location of the study area in the Colombian Caribbean, b) location of the virtual reanalysis buoys VB01 (10°40'1.12"N, 75°30'0.00"W) near Bocagrande and VB02 (11°30'N, 74°0'W) near Costa Verde, c) Bocagrande, Cartagena, d) Costa Verde, Ciénaga.

while Costa Verde is a microtidal reflective-intermediate beach.

Data processing and analysis

This research focused on the energy of G and IG waves and suspended sediment transport in the surf zone of microtidal reflective-intermediate and microtidal dissipative-intermediate beaches, using *in situ* instrumental data (Table 1). Bathymetric surveys were conducted during each climatic season to assess surf zone hydrodynamics (Ruiz-Merchán et al. 2019, 2025). The study focused on suspended-sediment transport in the upper-middle layer, using data from an Aquadopp Profiler operating in high-resolution (HR) mode, while excluding the region closest to the seabed because the instrument was mounted on a frame approximately 35 cm above the bottom (Fig. 2i), so the lowest region does not accurately represent flows in direct contact with benthic sediment. It could underestimate or distort near-bed sediment transport. Therefore, a region closer to the surface was selected, which, although not in direct contact with the seabed, provides a more dynamic and representative measurement of suspended sediment.

Pressure measurements were corrected for atmospheric pressure and converted to η using linear wave theory (Holthuijsen 2010). Significant wave heights (Hm_0) for both G and IG bands were then derived from these surface elevations.

The temporal resolution of the records varied between seasons. For the analysis of IG and G waves, as well as η and cross-shore (u) and alongshore (v) velocities, the resolution (1 Hz for 34 min h^{-1} in the dry season and 2 Hz for 17 min h^{-1} in the wet season) was sufficient to capture wave frequencies and amplitudes reliably. G and IG waves were separated using a Finite Impulse Response (FIR) band-pass filter, with cutoff ranges of 0.05-0.5 Hz for G waves and 0.0033-0.05 Hz for IG waves (Ruiz-Merchán et al. 2019). In contrast, backscatter data (counts), representing suspended sediment concentration, were averaged to a common temporal scale to ensure comparability across measurements obtained at different sampling frequencies (Aagaard & Greenwood 2008).

Correction of sediment backscatter data

Acoustic technology is an effective tool for measuring suspended sediment concentrations (Holdaway et al.

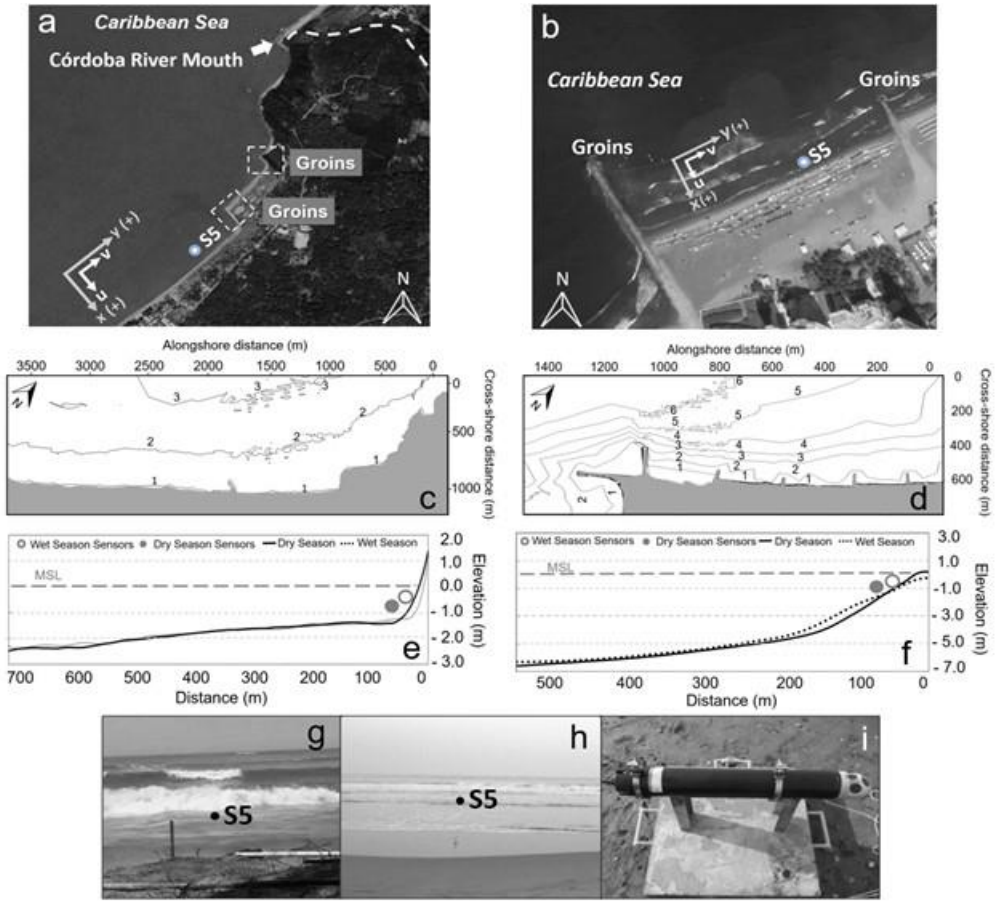

Figure 2. Plan view of the study area and equipment configuration (white velocity components *u* and *v* indicate positive values) a) Costa Verde Beach, b) Bocagrande Beach. Bathymetry of the study beaches: c) Costa Verde Beach, d) Bocagrande Beach. Beach profile and equipment configuration (dashed grey line represents mean sea level, MSL): e) Costa Verde Beach, f) Bocagrande Beach. Equipment location at Sensor 5 (S5): g) Costa Verde Beach, h) Bocagrande Beach, i) Aquadopp Profiler High Resolution (HR).

1999, Aagaard et al. 2013b). Due to its importance, acoustic backscatter intensity has been used to correct backscatter for surface sediment assessment (Sassi et al. 2012). Methods such as those applied by Aagaard & Greenwood (2008), who examined IG wave sediment transport in the surf zone, involved averaging data to a common temporal resolution to avoid biases resulting from differing sampling frequencies. Following this methodology, backscatter data were averaged to a common temporal scale to ensure comparability across measurements obtained at different sampling frequencies (1 Hz in the dry season and 2 Hz in the wet season). For consistency, the 2 Hz data were down-sampled to 1 Hz so that both datasets shared the same effective temporal resolution, thereby avoiding distortions in comparisons of general trends. To transform counts to sediment-corrected backscatter (SCB) values, the acoustic echo level (EL) equation must be used, as described by Lohrmann (2001). In other words, data from the measuring device, expressed in count units, are transformed into dB. In this regard, to transform from counts to SCB values, count values must be adjusted to a linear or logarithmic scale. In this way, measured values are expressed as a function of suspended particles, independent of depth. Therefore, it is important to apply a series of corrections to the backscatter signal, given the loss of intensity it experiences as it propagates through the water column:

$$EL = Couns \times\ 0.45 + 20Log_{10}(R) + 2\alpha_W R + 20R \int \alpha_p dr \quad (1)$$

where the terms correspond to:

(1) Conical shape of the acoustic beam: $Couns \times 0.45 + 20Log_{10}(R)$

(2) Acoustic wave absorption by water: $2\alpha_W R$

Table 1. Instrument configuration at Costa Verde and Bocagrande Beaches. Note: Details of the instrument configuration, including spatial resolution (m), temporal resolution (min, h), and frequency (Hz), for measuring cross-shore (*u*) and alongshore (*v*) currents, pressure, and acoustic backscatter (counts) during two climatic periods. The reported distances indicate the instrument's location relative to the shoreline.

Site beach type	Sensor	Sampling regime		Distance/Depth (m)		Variable	Zone
		Wet season	Dry season	Wet season	Dry season		
Costa Verde Beach Reflective intermediate	S5 Aquadopp HR	2 Hz 17 min h^{-1}	1 Hz 34 min h^{-1}	3/0.8	17/0.5	Currents (*u*, *v*), pressure and counts	Surf
Bocagrande Beach Dissipative intermediate	S5 Aquadopp HR	2 Hz 17 min h^{-1}	1 Hz 34 min h^{-1}	10/0.5	39/0.6	Currents (*u*, *v*), pressure and counts	Surf

(3) Acoustic energy scatter and absorption by suspended particles: $20R\int \alpha_p dr$

EL is the raw intensity of the acoustic backscatter signal recorded by the instrument, expressed in counts, before corrections for beam spreading and water absorption. The conversion factor between counts and backscatter intensity may vary within the range of 0,40 to 0,47 dB per count (Dwinovantyo et al. 2017); in this study, a value of 0,45 dB per count was adopted, which is valid as long as suspended sediment concentrations range between 1 and 10,000 mg L^{-1} (Lohrmann 2001, Sahin et al. 2017).

R is the range of the acoustic beam (m), α_w is the water absorption coefficient (dB m^{-1}), which varies between 1.2 and 1.6 for a device operating at 2 MHz (Clark et al. 2016), and αp is the particle attenuation coefficient (dB m^{-1}).

Terms 1-3 explain the EL intensity loss due to (a) acoustic scatter related to distance to the transmitter, (b) absorption by water, and (c) particle attenuation. According to Lohrmann (2001), the final term (3) can be ignored when suspended sediment concentrations are low, as it is small (Cartwright 2013). The amount of sediment in the surf zone varies between 0,4 and 1,4 g L^{-1} on dissipative beaches, reaching up to 6 g L^{-1} on intermediate beaches (Ibrahim 2005, Guerrero et al. 2024). Because of this, particle attenuation becomes very low (Lohrmann 2001), even though the surf zone features the largest sediment suspension values within the coastal strip due to the effect of wave breaking. Comparisons of surface suspended sediment with those in other environments (e.g. rivers or channels) reveal that the surf zone of a beach features low values of total suspended solids (TSS) (INVEMAR 2014). To calculate α_w, Equation 2 is applied, using the salinity and pressure values at the device depth, which are provided directly by the instrument.

where, $$a_w = \frac{A_1 P_1 F_1 f^2}{F_1^2+f^2} + \frac{A_2 P_2 F_2 f^2}{F_2^2+f^2} + A_3 P_3 f^2 \quad (2)$$

$$A_1 = \frac{8.86}{c} 10^{0.78pH-5} \quad (3)$$

$$A_2 = \frac{21.44S(1+0{,}025T)}{c} \quad (4)$$

$$A_3 = \left(4.937\times10^{-4}\right) - 2.59\times10^{-5}T - 9.11\times10^{-7}T^2 - 1.5\times10^{8}T^2 \quad (5)$$

$$F_1 = 2.8\left(\frac{S}{35}\right)^{0,5} \times 10^{4-\frac{1245}{\phi(T)}} \quad (6)$$

$$F_2 = \frac{8.17\text{x}10^{8-1990/(T+)}}{1+0.0018(S-35)} \quad (7)$$

$$P_1 = \left(1 - 3.93\times10^{-4}d\right) + 4.9\times10^{-10}d^2 \quad (8)$$

$$P_2 = 1 - 1.37\times10^{-4}d + 6.2\times10^{-9}d^2 \quad (9)$$

$$P_3 = 1 - 3.83\times10^{-5}d + 4.9\times10^{-10}d^2 \quad (10)$$

where T is water temperature in degrees Celsius, f is the emission frequency of the Aquadopp device, S is salinity, d is depth (m), and pH is the average alkalinity of the water column.

The speed of sound in water, c, is calculated using the following empirical relationship:

$$c = 1410 + 421T - 3.7T^2 + 110S + 0.18d \quad (11)$$

where T is the temperature (°C), S is the salinity, and d is the pressure or depth (m) at which the device is deployed. This equation depends on temperature, salinity, and pressure, as recorded by the instrument at a given depth (Lohrmann 2001).

In this study, the analysis was performed not on the seafloor but on the surface. In addition, sediment transport was quantified in relative rather than absolute terms. It is worth mentioning that even though term (3) is ignored in Equation 1, it is possible to make a precise physical interpretation of the results.

To analyze the contribution of IG waves to surf zone sediment transport, we applied the approach proposed

by Aagaard & Greenwood (2008). This method involves examining current velocity components (u, v) alongside suspended-sediment concentration fluxes to identify dominant frequencies and quantify the role of IG waves in advective sediment transport. Energy spectra and sediment flux cospectra were calculated to characterize the prevailing frequencies and directions of sediment transport within the IG frequency band.

Wavelet analysis

After obtaining the corrected sediment backscatter (SCB) data and combining them with the velocity components filtered in the IG and G frequency bands, sediment fluxes were computed for each season and integrated within each band to quantify their relative contributions to total transport. These fluxes, expressed in the time-frequency domain using the Continuous Wavelet Transform (CWT), allowed the identification of temporal variability in energy associated with G and IG.

The XWT was then applied between SCB fluxes and hydrodynamic variables (η, u, v) to examine common energy and phase relationships in the time-frequency domain. At the same time, WTC was used to assess the statistical significance of these relationships (Ruiz-Merchán et al. 2019). Arrows indicate phase relationships: arrows pointing right show in-phase behavior (0°), arrows pointing left indicate antiphase (180°), and vertical arrows represent a 90° phase difference upward arrows indicate the first series leads, and downward arrows indicate the second series leads. Areas of high coherence, represented by warm colors and aligned arrows, denote strong interdependence, suggesting that the variables are physically or dynamically related.

To ensure robust results, statistical significance levels were determined using Monte Carlo methods, following the approach described by Grinsted et al. (2004), which provides confidence limits for wavelet power, cross-wavelet spectra, and coherence values against red-noise backgrounds. This procedure ensured that the observed flux-hydrodynamic relationships in the G and IG frequency bands were not spurious correlations but reflected statistically reliable sediment transport dynamics.

To ensure full reproducibility of the wavelet-based analysis, all-time series were explicitly preprocessed and filtered. The velocity components (u, v) recorded with the Aquadopp HR Profiler underwent quality control, including median filtering to remove spikes and the exclusion of low signal-to-noise records. The G and IG wave bands were isolated using a Finite Impulse Response (FIR) band-pass filter with cutoff ranges of 0.05-0.5 Hz for G waves and 0.0033-0.05 Hz for IG waves (Ruiz-Merchán et al. 2019). SCB data were checked for anomalies, corrected for acoustic propagation losses, and temporally aligned with u, v, and η so that all variables shared a common time base. The resulting preprocessed series were then used in the CWT, XWT, and WTC analyses to characterize energy and sediment-flux variability in the IG and G bands. These procedures ensure that the wavelet-based analysis is robust, consistent, and fully reproducible with the available dataset.

RESULTS

This section presents the results of G and IG wave oscillation analyses, along with their relationships to surface elevation (η), current velocity components (u, v), and suspended sediment transport. Likewise, oscillations on two beaches (Costa Verde and Bocagrande) are identified, along with their impact on hydrodynamics and morphodynamics. Lastly, as a preliminary step for these analyses, the beaches studied herein are morphodynamically classified according to profile features, sediment type, and prevailing hydrodynamics.

Superficial suspended sediment fluxes.

SCB fluxes within the surf zone, both for the reflective-intermediate beach and the dissipative-intermediate beach are shown (Figs. 3-4). Autospectra (log-log scale). They were calculated from current velocity components (u, v, in grey), and SCB data were used to generate an SCB flux cospectrum (in black).

Figures 3a,c show that during the dry season, the u velocity component autospectrum was dominated by IG and G waves, with frequencies near f = 0.008 Hz (125 s) and f = 0.1 Hz (10 s), respectively. On the other side, the autospectrum plot of velocity component v features a significant IG signal, with frequencies ranging close to f = 0.015 Hz (64 s) and f = 0.005 Hz (180 s). Regarding the cospectral density of sediment, cross-shore and alongshore SCB fluxes featured frequencies close to f = 0.008 Hz (125 s), dominated by IG signal, exhibiting offshore and SW directions, and magnitudes close to -35 dB^2.

During the wet season, autospectrum plots Figures 3b,d provide evidence that the prevailing frequency in the v velocity component was 0.03 Hz (33 s), corresponding to IG waves. Likewise, frequencies between f = 0.02 Hz (50 s) and f = 0.007 Hz (128 s) were observed in the v velocity component

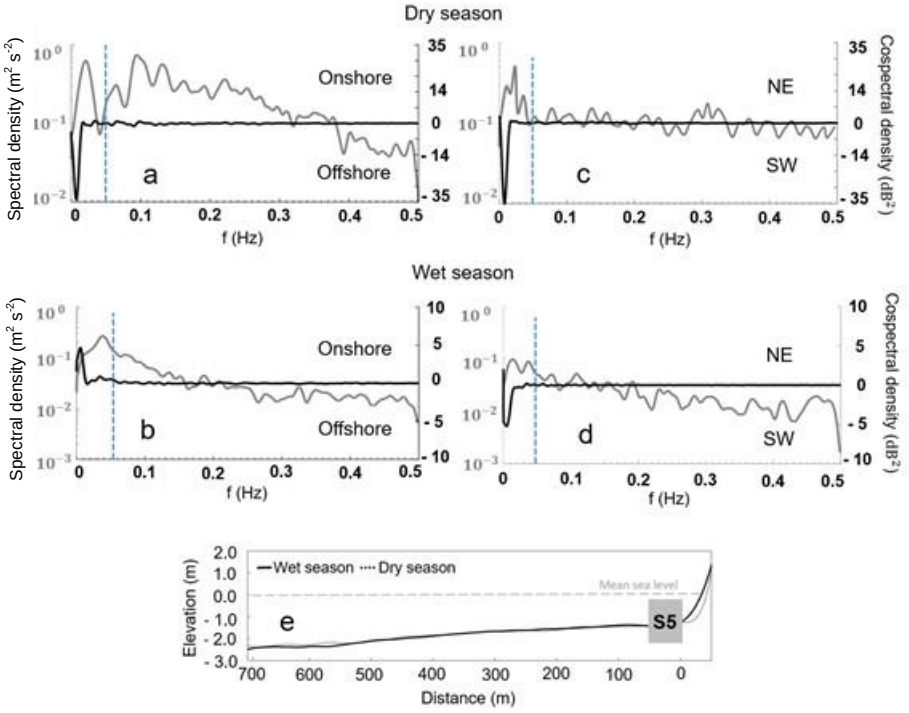

Figure 3. a-b) Auto-spectrum of cross-shore velocity *u* and c-d) alongshore velocity *v* [east-northeast (ENE) / west-southwest (WSW), gray], together with the cospectrum of sediment corrected backscatter (SCB, black), measured in the surf zone of the reflective-intermediate beach at Costa Verde. The velocity autospectra are shown in linear units: $m^2\ s^{-2}$ on the left Y-axis (gray), while the SCB cospectra are shown in logarithmic scale: dB^2 on the right Y-axis (black), both as a function of frequency f (Hz, X-axis). e) Beach profile. Panels a and c correspond to the dry season, and panels b and d to the wet season. The gray dotted line indicates the mean sea level (MSL), and the blue dotted line separates the infragravity (IG) wave signal from the gravity (G) wave signal.

autospectrum, predominantly in the IG regime. For SCB fluxes, they were detected at frequencies close to 0.02 Hz (50 s). In addition, cross-shore fluxes were directed onshore, and SW alongshore SCB fluxes featured magnitudes close to 5 dB^2 and -5 dB^2, respectively.

The autospectrum (log-log scale) of the velocity component *u* displayed two dominant signals corresponding to low- and high-frequency waves is shown (Fig. 4). The IG signal featured frequencies close to 0.01 Hz (100 s), and the G signal featured frequencies close to 0.1157 Hz (8 s). Nevertheless, for the autospectrum of the velocity component *v*, the IG signal exhibited frequencies of 0.02 Hz (50 s) and 0.04 Hz (25 s), with a larger signal than that of G waves. Regarding the cospectral density of sediment, cross-shore and alongshore SCB fluxes remained dominated by the IG regime with frequencies near f = 0.01 Hz (100 s). These SCB fluxes were directed onshore, with magnitudes close to -35 dB^2, and east-northeast (ENE) with intensities close to 5 dB^2.

During the wet season, Figures 4b,d reveal that the autospectrum of the velocity component *u* was influenced by frequencies f = 0.02 Hz (50 s) and f = 0.125 Hz (8 s), corresponding to the IG and G regimes, respectively. In contrast, the autospectrum of velocity component *v* featured frequencies between f = 0.009 Hz (111 s) and f = 0.5 Hz (2 s), which are within the frequency bands of IG and G, respectively. For the SCB cospectrum, the IG regime was evidenced to be dominant close to frequencies f = 0.009 Hz (111 s), confirming that cross-shore fluxes were onshore directed with values close to -15 dB^2, and alongshore fluxes in the west-southwest (WSW) direction, with magnitudes close to -11 dB^2. Cross-shore SCB fluxes featured magnitudes evidently larger than those of alongshore fluxes.

Wavelet analysis

Reflective-intermediate and dissipative-intermediate beaches were analyzed. The plots illustrate that most energy fluxes originated from IG frequencies, with

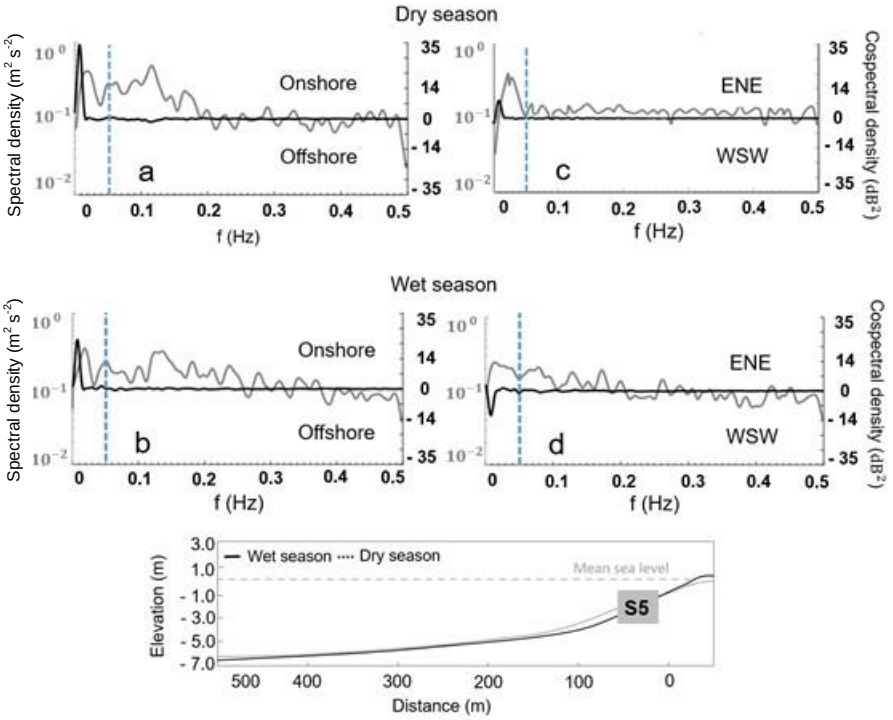

Figure 4. a-b) Auto-spectrum of cross-shore velocity *u*, and c-d) alongshore velocity *v* [east-northeast (ENE) / west-southwest (WSW), gray], together with the cospectrum of sediment corrected backscatter (SCB, black), measured in the surf zone of the dissipative-intermediate beach at Bocagrande. The velocity autospectra are shown in linear units: $m^2 s^{-2}$ on the left Y-axis (gray), while the SCB cospectra are shown in logarithmic scale: dB^2 on the right Y-axis (black), both as a function of frequency f (Hz, X-axis). e) Beach profile. Panels a and c correspond to the dry season, and panels b and d to the wet season. The gray dotted line indicates the mean sea level (MSL), and the blue dotted line separates the infragravity (IG) wave signal from the gravity (G) wave signal.

smaller contributions from G frequencies. The swell transported only small quantities of sediment, whereas the IG waves contributed significantly both in magnitude and direction.

Wavelet spectra were used to evaluate temporal variations in SCB within the surf zone at the location of sensor S5, allowing the identification of dominant SCB frequencies (Fig. 5). Likewise, the IG signal was evidenced to have influenced SCB during the dry season in both beaches (Fig. 5a,c). In fact, Costa Verde wave energy periods were consistently within the 32-520 s range, with a high level of significance in the 500-1,500 s interval. In Bocagrande, wave energy concentrated around periods ranging from 64-128 s, related to 200-800 s intervals. Nevertheless, in Bocagrande Beach, G energy showed a moderate, discontinuous significance near 8 and 16 s (Fig. 5c).

During the wet period, the presence of G and IG energies drives sediment transport on both beaches. However, in Costa Verde, the IG regime concentrated in periods between 32 and 64 s, displaying a high significance, and a very significant signal was also recorded for 128 s periods at 600 s. For Bocagrande beach, the G range had a greater influence on SCB than in Costa Verde. G signal periods ranged from 4 to 20 s, showing intermittency over time. IG signal periods ranged from 20 to 256 s and showed time discontinuities, with moderate to high significance. In addition, a very significant signal was observed between 200 and 800 s, with peaks at 64 and 128 s.

Figure 6 shows IG and G evolution in wavelet spectra for η and for current velocity components (u, v) during dry and wet seasons in the reflective-intermediate beach, recorded nearshore by sensor S5. During the dry season, η evidenced a significant contribution of G energy in 8 s and a significant IG signal in periods between 128 and 256 s during the 1,000-1,300 s interval. Nevertheless, moderate-energy discontinuities were observed in the IG periods between 64 and 128 s, for time intervals from 1,300 to

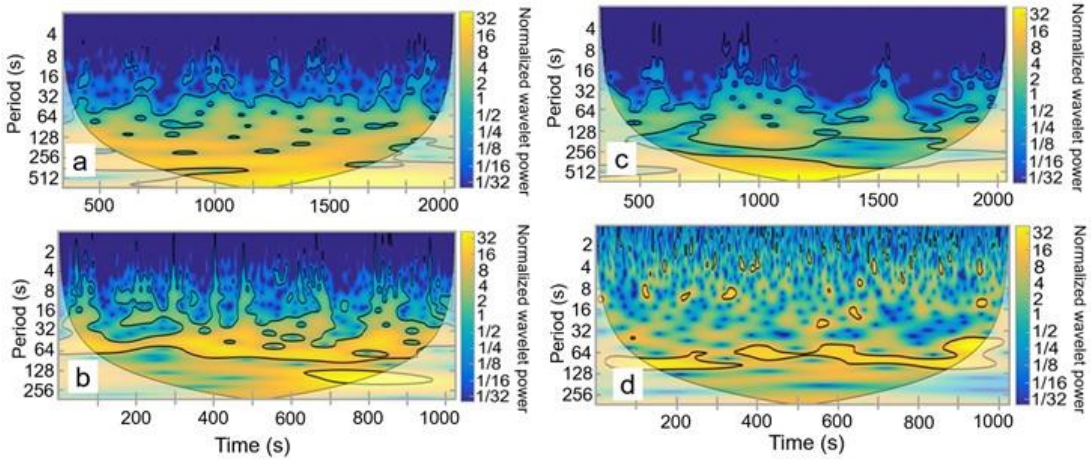

Figure 5. Continuous Wavelet Transform (CWT) representation of sediment corrected backscatter (SCB) in dB at a-b) Costa Verde, and c-d) at Bocagrande, with panels a and c representing the dry season and panels b and d representing the wet season.

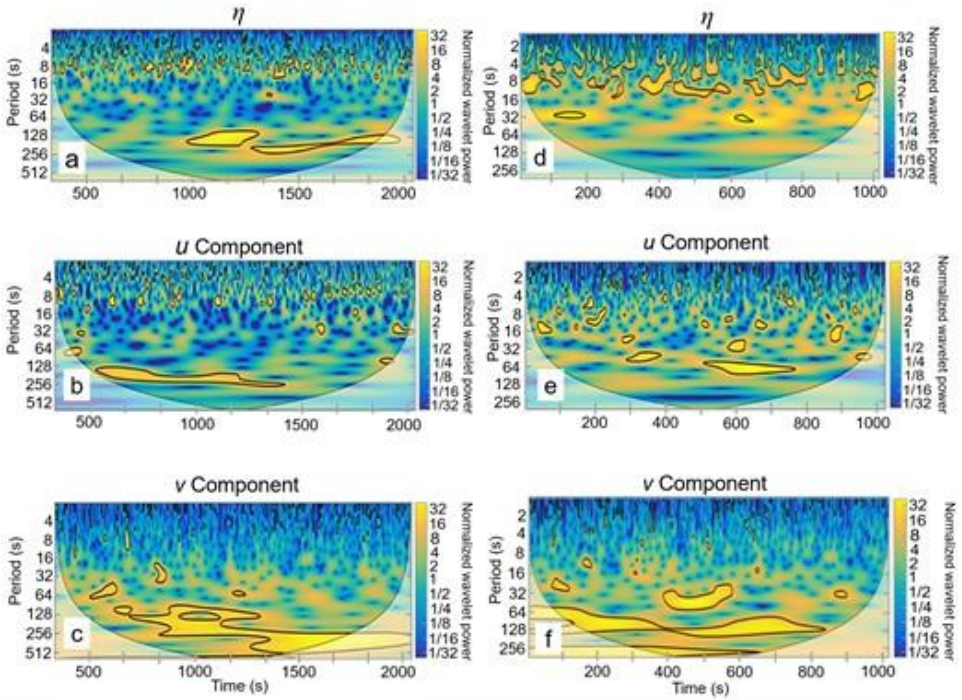

Figure 6. Continuous Wavelet Transform (CWT) representation at Costa Verde Beach showing a,d) free-surface elevation η, b,e) cross-shore current component u, and c,f) alongshore current component v. Panels a-c correspond to the dry season, while panels d-f correspond to the wet season.

1,700 s. During the wet season, η revealed that G energy was concentrated near 8-16 s, and IG energy was intermittently distributed in periods between 20 and 128 s, with a high coherence over a large time domain. Regarding the u velocity components of the wet and dry seasons, the G energy contribution was greater during the wet season. The IG signal contribution to u was more significant during the dry season, as the IG energy displayed high significance levels in periods close to 128 s in the interval between 500 and 1,300 s. For the case spectrum for the velocity components v, IG energy was dominant in the 64-256 s range, corresponding to the time intervals between 500 and 1,600 s, featuring high coherence levels.

Figure 7 shows results from the intermediate-dissipative beach, illustrating the evolution of η during the dry season, revealing that both G and IG energy are important. It is worth noting that IG energy was significant in the 128 s band during the 800 and 1,200 s intervals. On the other hand, G energy was dominant in periods near 8 s for most of the time domain. During the wet season, an IG signal was observed in the 32-256 s band, but the dominant signal was observed at 700 s in the time domain. For the velocity component *u*, spectra showed lower IG energy in the 32-128 s band during the wet season, with intermittent high-significance contributions, despite signal loss over time. This loss is attributed to energy dissipation from wave breaking in the *v*-component spectra. IG energy in the dry season was confirmed to prevail in the 64-256 s periods, with significant but discontinuous magnitudes during the 500-1,800 s time interval. In addition, for the wet-season spectrum, IG energy was present in the 20-64 s period, with discontinuities in the 300-800 s time interval. In contrast, G energy had little influence on *v* in both seasons.

Spectral XWT and WTC analyses for Costa Verde beach were based on sea states with Hmo = 0.91 m and Tp = 9.0 s during the dry season (Fig. 8). Even though XWT correlation was highly significant for the IG regime across the entire time domain, WTC correlation was confirmed only for specific periods. Highly significant correlations in XWT spectra were observed for the variable pairs η - SCB, *u* - SCB, and v - SCB, with a significant IG signal in the period range 64 to 512 s.

WTC spectra revealed that, during the dry season, coherence between η and SCB is intermittent, poorly defined, and low. Regarding the relationship between *u* and SCB, two dominant IG signals were observed. The first was recorded in periods close to 128 s, in the interval between 600 and 1,200 s, with a phase angle of 0°. The second IG signal was out of phase by 90°, with u dominant in periods near 256 s within the interval 400-1,000 s. For the relationship between *v* and SCB, IG was significant at periods near 128 s and in the interval 600-1,200 s, with a phase angle of 0°.

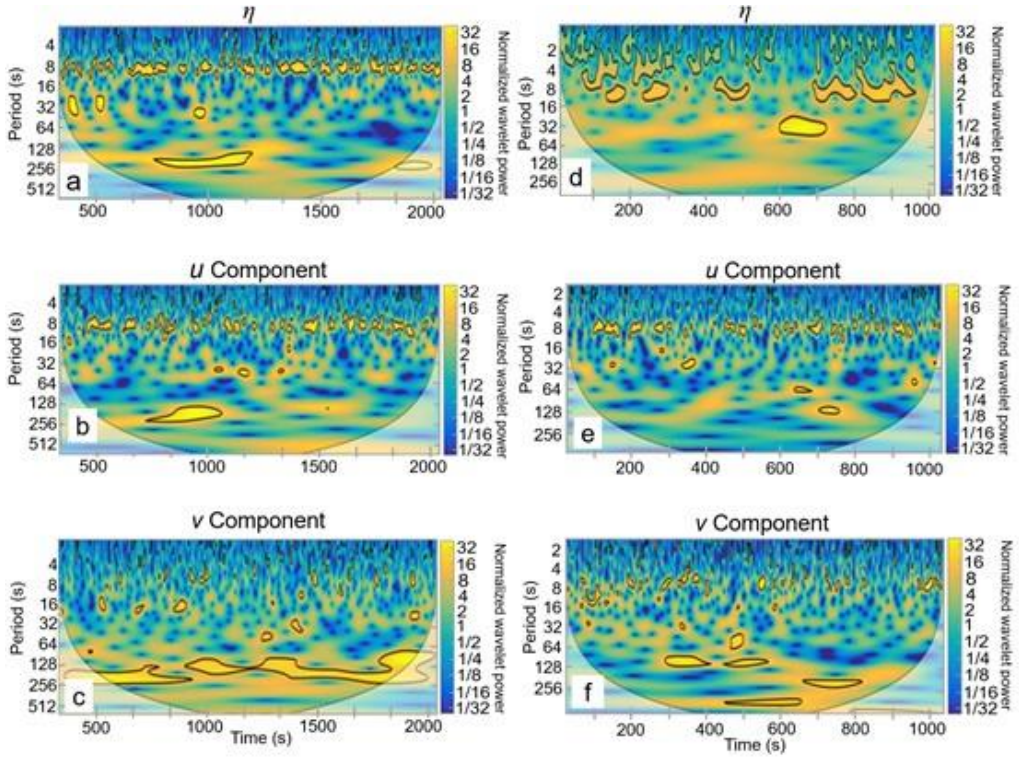

Figure 7. Continuous Wavelet Transform (CWT) representation at Bocagrande Beach showing a,d) free-surface elevation η, b,e) cross-shore current component *u*, c,f) and alongshore current component *v*. Panels a-c correspond to the dry season, while panels d-f correspond to the wet season.

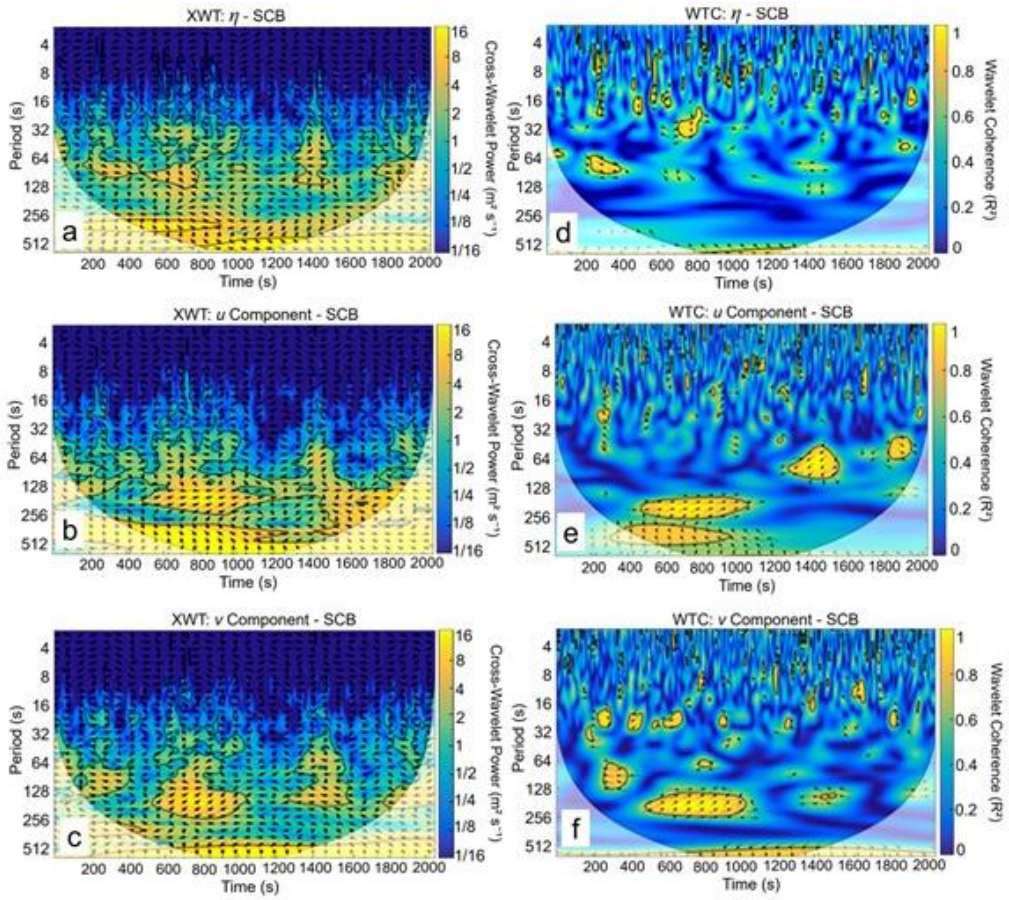

Figure 8. Cross Wavelet Transform (XWT) and Wavelet Transforms Coherence (WTC) spectra during the dry season on the reflective-intermediate beach. a) XWT of η-SCB, b) XWT of *u*-SCB, c) WTC of *v*-SCB, d) WTC of η-SCB, e) WTC of *u*-SCB, and f) WTC of *v*-SCB. Significant wave height Hmo = 0.91 m and peak period Tp = 9.0 s.

For XWT and WTC spectra during the wet season, sea states were close to Hmo = 0.72 m and Tp = 8.0 s (Fig. 9). Likewise, even though the G signal was moderate within wet season spectra, XWT correlation prevailed in the IG range through the entire time interval. The common signal revealed by WTC was observed only during specific, high-significance time intervals.

Coherence spectra for η-SCB featured a signal with values between 64 s with a phase angle of 0° and 128 s with a phase angle of 90°. In addition, an IG - dominated in phase signal was observed in the *u*-SCB spectrum for the 400-800 s interval. In terms of the *v*-SCB relationship, IG energies were dominant, with values recorded for periods between 64 and 128 s at 200 and 800 s, with phase angles of 0 and 90°, respectively. It implies that both variables will alternate between in-phase and out-of-phase states, with η leading SCB.

Figures 10-11 show XWT and WTC spectra, highlighting the relationships among SCB, η, *u*, and *v*, and their shared energies in the surf zone of Bocagrande beach, in both the dry and wet seasons. Observed sea states were close to Hmo = 0.75 m and Tp = 9.0 s during the dry season, whereas in the wet season, sea states ranged near Hmo = 0.36 m and Tp = 8.0 s.

XWT and WTC spectra during the dry season (Fig. 10) revealed that the relationship between η and SCB was highly significant for the 64 s periods, with both variables entering in phase at 900 s, then separating at 1,200 s, with η leading SCB. In this way, it was possible to infer that the angle of signal propagation changes through time. For spectra obtained during the dry season, the XWT spectrum showed that the *u*-SCB relationship had IG energy distributed discontinuously over the entire time interval. However, the signal most significant in XWT and WTC was found in the 128 and

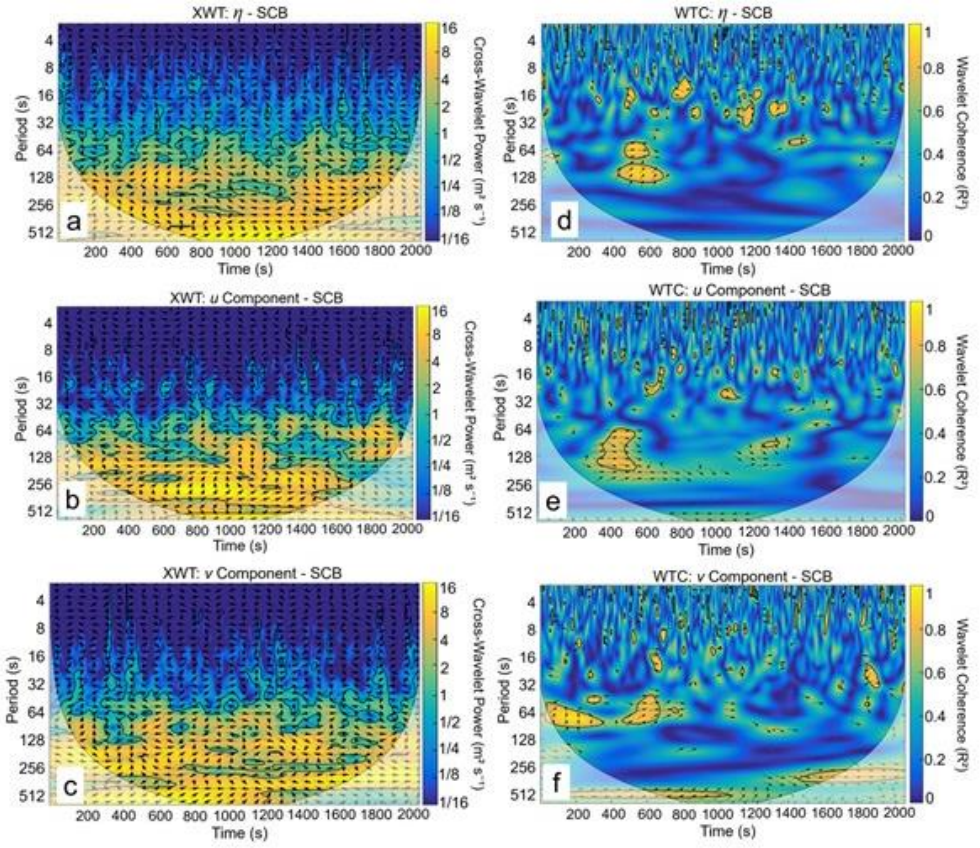

Figure 9. Cross Wavelet Transform (XWT) and Wavelet Transforms Coherence (WTC) spectra during the wet season on the reflective-intermediate beach. a) XWT of η-SCB, b) XWT of *u*-SCB, c) WTC of *v*-SCB, d) WTC of η-SCB, e) WTC of *u*-SCB, and f) WTC of *v*-SCB. Significant wave height Hmo = 0.72 m and peak period Tp = 8.0 s.

256 s periods, in the intervals between 800 and 1,400 s, with arrows predominantly directed to the right, and a phase angle of 0° for both variables, for the XWT and WTC spectra of the relationship between *v* and SCB, a high significance was obtained, with IG as the prevailing energy type in the periods between 64 and 128 s, corresponding to the intervals between 1,200 and 1,800 s. This pattern evidences that variables were in phase and oriented in the same direction.

Lastly, spectra obtained during the wet season (Fig. 11) indicated that G and IG energy were both significant in XWT. However, the IG remained the dominant signal in WTC spectra. For the relationship between η and SCB, shared energies were observed, with high significance in IG periods near 128 s, being out of phase at 180°, and moving in opposite directions. On the other hand, significant coherence values were also observed for the relationships *u*-SCB and *v*-SCB, with periods close to 128 s at intervals between 800 and 1,400 s, exhibiting a phase angle of 0°.

DISCUSSION

In this section, η, current velocity (*u*, *v*), and SCB data from reflective-intermediate and dissipative-intermediate beaches during the dry and wet seasons are analyzed, and the resulting patterns are discussed. Specifically, we examine (i) the propagation of infragravity (IG) wave energy, (ii) the evolution of gravity (G) wave energy as swells approaches the shoreline, (iii) the interaction between G and IG energy, (iv) the associated current-velocity fields within the surf zone, and (v) the corresponding SCB patterns in the study area. Because these analyses quantify co-variability and phase relationships, we explicitly distinguish robust associations from direct causation when interpreting the results.

The statistical tools applied here (autospectra/ cospectra, CWT, XWT, and WTC) quantify time-frequency co-variability and phase relationships between free-surface elevation (η), currents (*u*, *v*), and corrected sediment backscatter (SCB). Importantly,

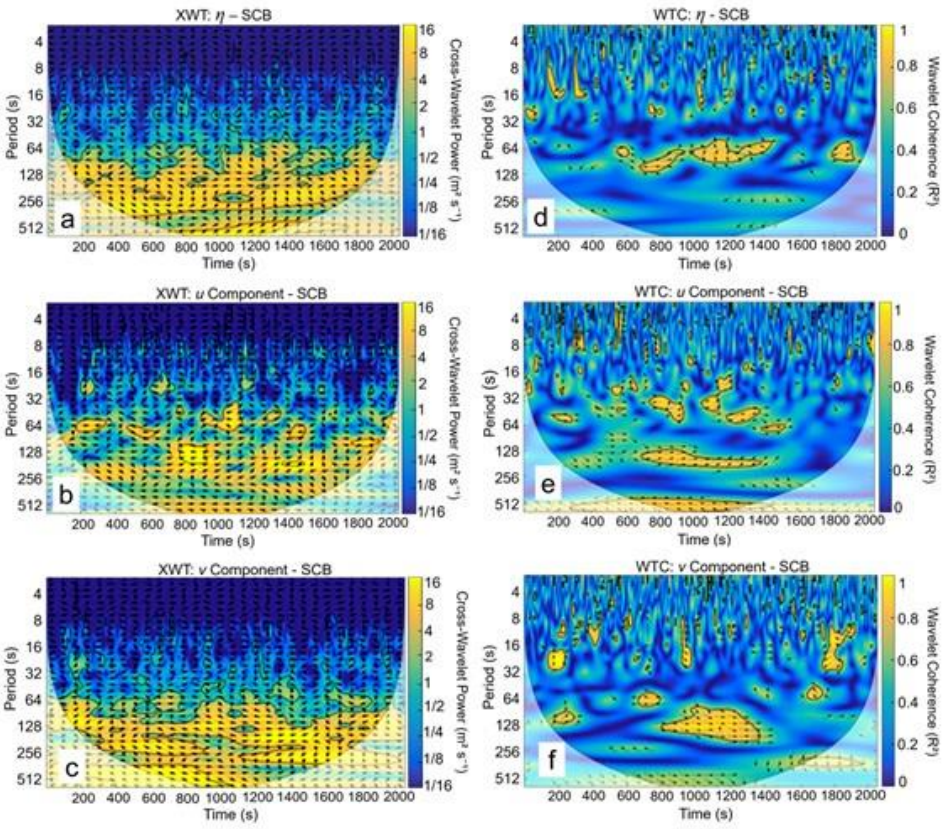

Figure 10. Cross Wavelet Transform (XWT) and Wavelet Transforms Coherence (WTC) spectra during the dry season on the dissipative-intermediate beach at Bocagrande. Panels show: a) XWT of η-SCB, b) XWT of u-SCB, c) WTC of v-SCB, d) WTC of η-SCB, e) WTC of u-SCB, and f) WTC of v-SCB. Significant wave height Hmo = 0.75 m and peak period Tp = 9.0 s.

coherence and cross-wavelet power indicate robust association rather than direct causation by themselves; therefore, causal language in this study is used in a process-based sense, supported by (i) established hydrodynamic mechanisms linking infragravity (IG) motions to surf-zone currents and advection, (ii) the convergence of independent diagnostics showing dominant IG signatures in sediment-flux patterns, and (iii) the consistent lead-lag/phase behavior observed between forcing variables (η, u, v) and SCB fluxes at IG periods. Statistical significance for wavelet power and coherence was evaluated against red-noise backgrounds using Monte Carlo confidence limits, which reduces the likelihood that the reported relationships arise from spurious correlations. In addition, although a formal parametric sensitivity analysis is beyond the scope of the present dataset, the key interpretation-IG dominance in nearshore sediment transport-remains consistent across seasons, across both cross-shore and alongshore components, and across the two contrasting beach states. Finally, the inferred transport directions are morphologically plausible because at Costa Verde, nearshore reflection and IG-driven edge-wave dynamics are consistent with cusp-related sediment redistribution and with the influence of groins and seasonal riverine sediment supply; at Bocagrande, onshore-directed IG fluxes during lower-energy conditions are consistent with convex-profile/berm development and the seasonal modulation of cusp expression.

Suspended sediment fluxes

In the surf zone, sediments are strongly suspended from the bottom and transported in u and v directions, leading to morphological changes in beach areas (de Bakker 2016). In addition, IG waves may dominate sediment transport within the surf zone and, under energetic conditions, may be responsible for beach erosion (Russell 1993) and sediment accumulation (de Vries et al. 2008), and may eventually induce beach flooding.

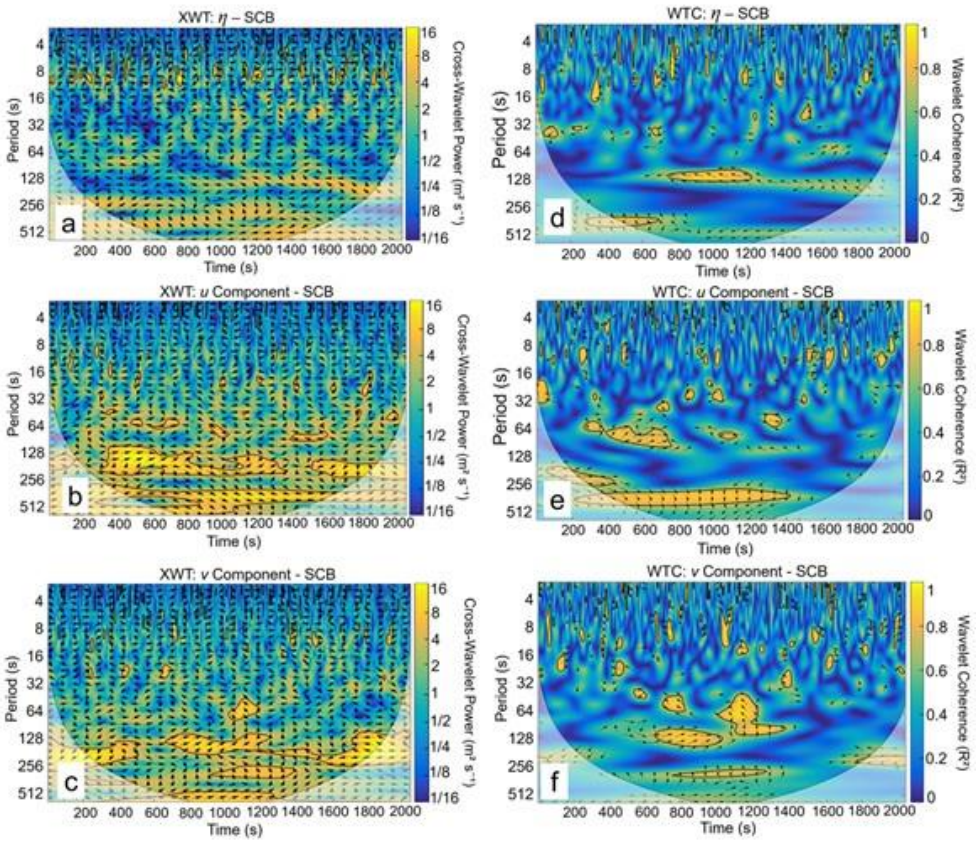

Figure 11. Cross Wavelet Transform (XWT) and Wavelet Transforms Coherence (WTC) spectra during the wet season on the dissipative-intermediate beach at Bocagrande. a) XWT of *η*-SCB, b) XWT of *u*-SCB, c) WTC of *v*-SCB, d) WTC of *η*-SCB, e) WTC of *u*-SCB, and f) WTC of *v*-SCB. Significant wave height Hmo = 0.36 m and peak period Tp = 8.0 s.

Estimates of cross-shore and alongshore SCB flux (Figs. 3-4) were essential for predicting sediment movement direction and, therefore, for identifying dominant frequencies under moderate and energetic conditions.

During the dry season, in the reflective-intermediate beach, offshore SCB fluxes were produced in the IG regime (Fig. 3a). This pattern coincides with the work of Brinkkemper et al. (2013), who pointed out that the most energetic offshore-directed swells are associated with greater IG energies. Cross-shore SCB fluxes move in an offshore direction in Costa Verde, indicating a reflection very close to the shoreline. These fluxes sometimes form edge waves, which are responsible for cusp formation on the beach, sediment transport, and erosive phenomena (Ruiz-Merchán et al. 2019). In this sense, it can be inferred that, in a certain way, offshore sediment transport in Costa Verde is compensated by sediments transported onshore (Aagaard et al. 2013a).

For the wet season (Fig. 3b), cospectral values were positive in Costa Verde, indicating that cross-shore SCB fluxes are onshore directed, showing a maximum energy concentration in the IG frequency (0.004 Hz). The above implies that IG energy dominates accretion processes on the beach. On the other hand, sediment accretion on this beach is also influenced by the Cordoba River (Fig. 2a). In addition to the groins, a small Cordoba River delta with highly complex dynamics was observed in the study zone. During the wet season, sediment influx from rivers in the Colombian Caribbean increases significantly, as these rivers experience sudden, short-term swellings triggered by heavy rainfall events. These rapid increases in discharge enhance rivers' capacity to transport sediment towards the coast, contributing to the sediment budget of beaches such as Costa Verde (Escobar & Velasquez-Montoya 2018). In contrast, during the dry season, most of the hydrological cycle has a low-magnitude base flow, in which virtually no sediment transport is produced (INVEMAR 2017)

The IG regime dominates alongshore SCB fluxes, which are negative to the SW direction (Fig. 3c-d),

indicating that sediment is transported in the SW direction, both in the dry and wet seasons, under the influence of IG energy. This sediment transport, together with the energetic swell present in the zone, may be associated with erosive processes. In addition to this, the presence of groins disrupts any sediment supply that might compensate for the imbalance caused by energetic swell in the beach. These results are consistent with those reported by INVEMAR 2006, 2017, indicating that Costa Verde featured a very energetic swell. As a result, intense erosive processes have been reported after groins are installed, indicating that groins accelerate erosion and contribute to beach retreat.

From a beach-erosion perspective related to groins, INVEMAR (2017) reported that significant erosion occurred in the infratidal zone. These processes are a warning sign of sediment loss due to coastal transport and the absence of depositional events that would allow a positive sediment balance, leading to coastline retreat. On the other side, (Rangel-Buitrago et al. 2015) show that Costa Verde groins, despite affecting velocities nearshore, do not appear to affect sedimentary dynamics under energetic swell conditions. Nevertheless, Montaño-Muñoz et al. (2018) revealed, using *in situ* data, rapid coastline retreat in Costa Verde after the groin was built, due to the disruption of sediment supply, which affected nearshore current velocities (u, v).

On Bocagrande beach, during the dry season (Fig. 4b), positive cospectral values in the IG regime indicated that, under energetic conditions, cross-shore SCB flux has an onshore direction. The latter evidences the influence of IG energy on the water sheet, which lasts longer in dry areas. In addition, the berm formed during the wet season eroded, likely due to IG energy dissipation along the beach profile. According to Conde-Frías et al. (2017), the dynamics of dissipative, microtidal beaches in the Colombian Caribbean, in which IG energy does not dissipate on the swash and surf zones, is an extension of a water sheet that is more extended over dry areas. The latter was related by the same authors to transport, as a hydrodynamic response more visible in energetic swell conditions on microtidal, dissipative beaches. According to Márquez et al. (1998) and Rangel-Buitrago et al. (2015), under energetic conditions, beaches acquire a gentle slope resulting from erosion, becoming zones easily exposed to flooding, particularly affecting areas of touristic development. In addition, during the dry season in Bocagrande, a concave beach profile is generated, revealing signs of erosion. These results are consistent with the studies by Márquez et al. (1998) on beaches in the Colombian Caribbean. During the wet season, on the dissipative-intermediate beach (Fig. 4b), cross-shore SCB fluxes were directed toward the shore, with peak energy occurring at IG frequencies. These results align with (Ruessink 1998), who observed that IG waves amplify onshore as free waves during periods of reduced overall energy. This result is expected, given that during the wet season, due to moderate swell energy, the beach profile becomes convex (Fig. 2f). Under these conditions, sediment accumulation occurs, leading to berm formation and clearly marking the limit of the dry zone (Ruiz-Merchán et al. 2025).

Bocagrande beach is located between two rocky groins intended to stabilize it. Therefore, the beach's capacity to retain sediments during the dry and wet seasons directs cross-shore SCB fluxes onshore. During the wet season, alongshore fluxes are negative and directed WSW, corresponding to IG frequencies, which implies that sediment transported along the coastline will show signs of erosion. The opposite happens during the dry season, with energetic conditions, when alongshore SCB fluxes are positive and oriented towards the ENE. This scenario leads to a distribution of sand transportation through the surf zone parallel to the coast.

Bocagrande is a dissipative-intermediate beach. Therefore, due to their intermediate condition, cups often appear on the beach as IG waves become trapped during the dry season (Ruiz-Merchán et al. 2025). However, during the wet season, *cusp* disappearance can be attributed to the development of a continuous berm along the coast or to extreme events. These results agree with those presented by Almar et al. (2008).

At Costa Verde and Bocagrande, sediment transport driven by SCB fluxes within the IG wave regime corresponds with (Cueto & Otero (2020), who found that high-energy IG wave fluxes move offshore on reflective beaches and onshore on dissipative or intermediate beaches. This energy-based behavior aligns with the results observed at Costa Verde, where, during the dry season, IG energy fluxes are directed offshore, promoting erosive processes (Fig. 3a), and at Bocagrande, during the wet season, fluxes are directed onshore, promoting sediment accumulation (Fig. 4b).

Cueto & Otero (2020) and Cueto et al. (2022) highlight that IG energy flux magnitudes control both the direction and intensity of sediment transport; this is reflected in seasonal dynamics at Bocagrande, where higher IG energy during the dry season corresponds to significant erosion and alongshore sediment redistribution. (Fig. 4a), whereas during the wet season, when

swell energy is lower, accretion processes are favored. These findings are also supported by Montaño-Muñoz et al. (2018), who, based on in situ measurements, reported rapid shoreline retreat at Costa Verde following the construction of groins. This retreat was attributed to sediment supply interruptions and modifications in nearshore current velocities (u, v), processes that are amplified under energetic IG wave forcing. Thus, the empirical evidence presented by both Montaño-Muñoz et al. (2018) and Cueto & Otero (2020) complements the SCB cospectral patterns described in this study, providing a broader energy-based perspective that reinforces the seasonal morphodynamic interpretation of both beaches.

Wavelet analysis

Wavelet analysis provided a complementary approach to SCB flux analysis, allowing identification of the energy distribution and its relationship with η, u, and v as forcings of sediment suspension. The wavelet energy spectra (CWT) revealed that low-frequency motions, especially within the IG regime, directly contributed to sediment suspension in both dry and wet seasons. Notably, the IG energy dominated the spectra of current velocities (u, v), reinforcing its key role in SCB processes.

Analyses using XWT and WTC revealed that both G and IG energies, which directly influence SCB hydrodynamics, were higher during the dry season, particularly at the dissipative-intermediate beach compared with the reflective-intermediate beach. These spatial and seasonal changes are attributed to sediment grain size and wave-breaking types. While (Kana (1978) argued that plunging waves suspend more sediment than spilling waves, our results suggest the opposite: in Bocagrande, finer sediments were more easily suspended by spilling breakers. This finding aligns with Cueto & Otero (2020), who emphasized that the magnitude and direction of IG energy fluxes are critical in controlling sediment transport, especially on dissipative to intermediate beaches, where onshore-directed IG fluxes are enhanced during lower-energy (wet) conditions.

At Costa Verde, XWT and WTC spectra during the dry season showed a 0° phase angle between u-SCB and v-SCB, with coherence values near 1, indicating a strong, in-phase relationship. These currents act as dominant drivers of sediment transport, supported by the presence of cross-shore and standing leaky and edge waves alongshore. During the wet season, u and v remained strongly in phase, while a 90° phase shift between η and SCB indicates the influence of progressive leaky IG waves in both cross-shore and alongshore directions (Ruessink 1998, Aagaard & Greenwood 2008), supporting the idea that under moderate conditions, progressive IG waves may dominate nearshore sediment dynamics.

At Bocagrande during the dry season, η, u, and v were largely in phase with SCB, indicating coherent energy and sediment responses; however, a 90° phase shift between η and SCB at 64-256 s suggests η as the dominant forcing. This pattern points to the influence of standing edge waves, consistent with Winter et al. (2017) and Montaño-Muñoz et al. (2018), who showed that standing IG waves can develop in coasts with irregular bathymetry or human-made structures such as groins or rocky outcrops. These structures can generate partial-wave reflection, thereby enhancing nearshore IG energy and facilitating the development of beach cusps and zones of increased sediment suspension.

During the wet season, phase relationships between variables were more variable. Sediment transport was likely influenced by standing edge waves trapped between groins, promoting cusp formation, consistent with Montaño-Muñoz et al. (2018) and Ruiz-Merchán et al. (2019), who observed edge waves trapped nearshore in Costa Verde. Similarly, Gallagher (1971) showed that reflected G-waves can refract and become trapped as edge waves. Cueto & Otero (2020) further explain these dynamics, showing that on dissipative or intermediate beaches, IG energy fluxes typically move onshore under moderate wave conditions, leading to sediment buildup. This pattern was seen at Bocagrande in the wet season.

Additionally, leaky waves propagating cross-shore and progressive waves moving alongshore contributed to sediment transport. Of particular importance are the currents (u, v) under IG energy, which facilitate advection of suspended sediments-potentially the dominant mechanism shaping surf zone morphodynamics (Bowen & Huntley 1984). Future field deployments, especially with alongshore-distributed sensors, are needed to verify whether advection, particularly via the v component, plays a leading role in sediment redistribution.

CONCLUSION

The analysis using XWT and WTC proved effective in identifying the relationship between IG wave energy and suspended sediment transport, allowing the detection of both general patterns and site-specific differences. The main findings are summarized as follows:

- IG waves play a key role in suspended sediment transport and morphodynamic changes in both reflective-intermediate and dissipative-intermediate beach systems.
- At the studied sites, IG energy consistently dominates in the nearshore zone, while G wave contributions to sediment fluxes remain limited.
- The intensity, direction, and seasonal variations of sediment transport are mainly controlled by beach type, sediment grain size, wave-breaking patterns, and prevailing climatic conditions.
- The interaction between IG waves and beach morphology governs patterns of erosion and sediment deposition.
- At Costa Verde, alongshore SCB fluxes indicate persistent erosive tendencies, exacerbated by limited sediment input from fluvial sources and the presence of groin structures.
- At Bocagrande, cross-shore SCB fluxes favor onshore sediment accumulation, with seasonal shifts in flux direction linked to groins, which enhance sediment retention during the wet season but can also induce alongshore transport and localized erosion.
- Edge and leaky IG wave patterns are key in driving both cross-shore and alongshore sediment movements.
- Current velocities associated with IG waves (u, v) are the primary driver of sediment advection and redistribution, especially under low- to moderate-energy conditions.
- The results show that IG waves are the main drivers of sediment transport and morphodynamic changes in the nearshore zone, creating clear areas of erosion and deposition that vary seasonally. Quantitative patterns of cross-shore and alongshore fluxes allow prediction of sediment movement under different energy conditions, providing valuable information for coastal management. Understanding these dynamics is essential for planning and designing interventions such as beach nourishment, erosion mitigation, and coastal infrastructure, ensuring that actions align with natural sediment pathways and minimize unwanted impacts on shoreline stability. Future studies should consider the influence of riverine sediment supply, particularly during high discharge periods in the wet season, as this can significantly affect nearshore sediment dynamics and coastal management strategies.

Credit author contribution

J.K. Ruiz-Merchán contributed to conceptualization, validation, methodology, formal analysis, writing of the original draft review and editing; B.K. Haus contributed to formal analysis and review; J.C. Restrepo, L. Otero, J. Cueto, and M. Conde-Frías: conceptualization, validation, methodology, formal analysis, writing of the original draft and review; M. Guerrero, S. Henriquez, J.M. Rebellón and A. Guerrero: data curation, formal analysis, and review. All authors have read and approved the final version of the manuscript.

Conflicts of interest

The authors declare no conflicts of interest.

Data availability statement

The data presented in this study are available on request from the corresponding author.

ACKNOWLEDGMENTS

The authors thank the Ministerio de Ciencia, Tecnología e Innovación and The Alfred C. Glassell Jr. SUSTAIN (Surge-Structure-Atmosphere Interaction) Laboratory for the financial support. The authors also thank the Department of Research, Development, and Innovation at the Universidad del Norte and the Reef Institute.

REFERENCES

Aagaard, T. & Greenwood, B. 2008. Infragravity wave contribution to surf zone sediment transport -The role of advection. Marine Geology, 251: 1-14. doi: 10.1016/j.margeo.2008.01.017

Aagaard, T., Greenwood, B. & Hughes, M. 2013a. Sediment transport on dissipative, intermediate and reflective beaches. Earth-Science Reviews, 124: 32-50. doi: 10.1016/j.earscirev.2013.05.002

Aagaard, T., Greenwood, B. & Larsen, S.M. 2013b. Total cross-shore sediment transport under shoaling waves on a steep beach. Proceedings of Coastal Dynamics, 2013: 39-50.

Almar, R., Coco, G., Bryan, K., et al. 2008. Video observations of beach cusp morphodynamics. Marine Geology, 254: 216-223.

Andrade, C., Thomas, A., Lerma, A., et al. 2013. Coastal flooding hazard related to swell events in Cartagena de Indias, Colombia. Journal of Coastal Research, 29: 1126-1136.

Auer, F., Ahmerkamp, S., Cueto, J., et al. 2025. Extensive oxygen consumption in the intertidal infiltration zone of beach aquifers-the impact of seasonal input, filtration efficiency, and morphodynamics. Journal of Geophysical Research: Biogeosciences, 130: e2024JG 008291. doi: 10.1029/2024JG008291

Austin, M. & Masselink, G. 2006. Observations of morphological change and sediment transport on a steep gravel beach. Marine Geology, 229: 59-77. doi: 10.1016/j.margeo.2006.02.003

Baldock, J., Masiello, C., Gelinas, Y., et al. 2004. Cycling and composition of organic matter in terrestrial and marine ecosystems. Marine Chemistry, 92: 39-64. doi: 10.1016/j.marchem.2004.06.016

Bowen, A. & Huntley, D. 1984. Waves, long waves and nearshore morphology. Marine Geology, 60: 1-13.

Brinkkemper, J., Torres-Freyermuth, A., Mendoza, E., et al. 2013. Parameterization of wave run-up on beaches in Yucatan, Mexico: A numerical study. Proceedings of Coastal Dynamics, 2013: 225-234.

Cartwright, G. 2013. Application of acoustics and optics for the characterization of suspended particulate matter within an estuarine observing system. The College of William and Mary, Virginia.

Clark, M., Consalvey, M. & Rowden, A. 2016. Biological sampling in the deep sea. John Wiley & Sons, New York.

Conde-Frías, M., Otero, L., Ortiz, J., et al. 2017. Swash oscillations in a microtidal dissipative beach. Journal of Coastal Research, 336: 1408-1422. doi: 10.2112/JCOASTRES-D-16-00147.1

Cueto, J. & Otero, L. 2020. Morphodynamic response to extreme wave events of microtidal dissipative and reflective beaches. Applied Ocean Research, 101: 102283.

Cueto, J., Otero, L., Ospino-Ortiz, S., et al. 2022. The role of morphodynamics in predicting coastal flooding from storms on a dissipative beach with sea level rise conditions. Natural Hazards and Earth System Sciences, 22: 713-728. doi: 10.5194/nhess-22-713-2022

de Bakker, A. 2016. Infragravity-wave dynamics in shallow water: energy dissipation and role in sand suspension and transport. Dissertation, Utrecht University, Utrecht.

de Vries, J.S.M., van Gent, M.R.A., Walstra, D.-J., et al. 2008. Analysis of dune erosion processes in large-scale flume experiments. Coastal Engineering, 55: 1028-1040.

Dwinovantyo, A., Manik, H., Prartono, T., et al. 2017. Quantification and analysis of suspended sediments concentration using mobile and static acoustic doppler current profiler instruments. Advances in Acoustics and Vibration, 2017: 1-14. doi: 10.1155/2017/4890421

Elgar, S., Gallagher, E. & Guza, R. 2001. Nearshore sandbar migration. Journal of Geophysical Research: Oceans, 106: 11623-11627. doi: 10.1029/2000JC000389

Escobar, C. & Velasquez-Montoya, L. 2018. Modeling the sediment dynamics in the Gulf of Uraba, Colombian Caribbean Sea. Ocean Engineering, 147: 476-487.

Feddersen, F., Guza, R., Elgar, S., et al. 2000. Velocity moments in alongshore bottom stress parameterizations. Journal of Geophysical Research: Oceans, 105: 8673-8686.

Gallagher, B. 1971. Generation of surf beat by non-linear wave interactions. Journal of Fluid Mechanics, 49: 1-20.

Garcia, F., Palacio, C. & Garcia, U. 2011. Tide constituents at Santa Marta Bay (Colombia). Dyna, 78: 142-150.

Goodfellow, B. & Stephenson, W. 2008. Role of Infragravity energy in bar formation in a strong-wind bay: observations from Seaford Beach, Port Phillip Bay, Australia. Geographical Research, 46: 208-223. doi: 10.1111/j.1745-5871.2008.00511.x

Grinsted, A., Moore, J. & Jevrejeva, S. 2004. Application of the cross wavelet transform and wavelet coherence to geophysical time series. Non-linear Processes in Geophysics, 11: 561-566. doi: 10.5194/npg-11-561-2004

Guerrero, A., Otero, L., Ospino, S., et al. 2024. Interactions between hydrodynamic forcing, suspended sediment transport, and morphology in a microtidal intermediate-dissipative beach. Journal of Marine Science and Engineering, 12: 1141. doi: 10.3390/jmse12071141

Guza, R. & Thornton, E. 1982. Swash oscillations on a natural beach. Journal of Geophysical Research, 87: 483-491. doi: 10.1029/JC087iC01p00483

Holdaway, G., Thorne, P., Flatt, D., et al. 1999. Comparison between ADCP and transmissometer measurements of suspended sediment concentration. Continental Shelf Research, 19: 421-441.

Holman, R. 1981. Infragravity energy in the surf zone. Journal of Geophysical Research: Oceans, 86: 6442-6450. doi: 10.1029/JC086iC07p06442

Holthuijsen, L. 2010. Waves in oceanic and coastal waters. Cambridge University Press, Cambridge. doi: 10.1017/CBO9780511618536

Hsu, T.-J. & Hanes, D. 2004. Effects of wave shape on sheet flow sediment transport. Journal of Geophysical Research: Oceans: 109: 002075. doi: 10.1029/2003JC002075

Huntley, D. & Bowen, A. 1973. Field observations of edge waves. Nature, 243: 160-162. doi: 10.1038/243160a0

Ibrahim, J. 2005. Morphodynamics and surf zone sediment transport for two beaches in Trinidad: Response to wet and dry seasons. Journal of Coastal Research, 21: 294-302.

Instituto de Investigaciones Marinas y Costeras de Colombia (INVEMAR). 2006. Programa de prevención y propuestas de mitigación de la erosión costera en Colombia. Fase I. Proyecto BPIN Diagnóstico de la erosión costera en el Caribe. INVEMAR, Santa Marta.

Instituto de Investigaciones Marinas y Costeras de Colombia (INVEMAR). 2014. Informe del estado de los ambientes y recursos marinos y costeros en Colombia. INVEMAR, Santa Marta.

Instituto de Investigaciones Marinas y Costeras (INVEMAR). 2017. Evaluación de las condiciones ambientales de la zona marino-costera del departamento del Magdalena como herramienta para la gestión ambiental de CORPAMAG. Informe técnico final. INVEMAR, Santa Marta.

Kana, T. 1978. Surf zone measurements of suspended sediment. Coastal Engineering, 1978: 1725-1743.

Kjerfve, B. 1981. Tides of the Caribbean Sea. Journal of Geophysical Research, 86: 4243-4247. doi: 10.1029/JC086iC05p04243

Lohrmann, A. 2001. Monitoring sediment concentration with acoustic backscattering instruments. Nortek Technical Note No. 003, Document No. N4000-712. Nortek AS, Rud. [https://www.nortekgroup.com/assets/documents/Monitoring-sediment-concentration-with-acoustic-backscattering-instruments.pdf]. Reviewed: March 31, 2026.

Longuet-Higgins, M. & Stewart, R. 1962. Radiation stress and mass transport in gravity waves, with application to surf beats. Journal of Fluid Mechanics, 13: 481-504.

Longuet-Higgins, M. & Stewart, R. 1964. Radiation stresses in water waves: a physical discussion, with applications. Deep Sea Research and Oceanographic Abstracts, 11: 529-562.

Márquez, A., Ospina, L. & Márquez, L. 1998. Variaciones morfológicas y texturales de las playas entre Barranquilla y flecha de Galerazamba (1935-1996). Boletín Científico CIOH, 18: 23-38.

Montaño-Muñoz, J., Osorio, A. & Otero, L. 2018. Patrones en las excursiones de swash en dos playas contrastantes: Playas Hollywood y Costa Verde, Colombia. Dyna, 85: 264-271.

O'Donoghue, T. & Wright, S. 2004. Concentrations in oscillatory sheet flow for well sorted and graded sands. Coastal Engineering, 50: 117-138. doi: 10.1016/j.coastaleng.2003.09.004

Péquignet, A., Becker, J., Merrifield, M., et al. 2009. Forcing of resonant modes on a fringing reef during tropical storm Man-Yi. Geophysical Research Letters, 36: 2008GL036259. doi: 10.1029/2008 GL036259

Rangel-Buitrago, N., Anfuso, G. & Williams, A. 2015. Coastal erosion along the Caribbean coast of Colombia: Magnitudes, causes and management. Ocean & Coastal Management, 114: 129-144.

Restrepo, J., Otero, L., Casas, A., et al. 2012. Shoreline changes between 1954 and 2007 in the marine protected area of the Rosario Island Archipelago (Caribbean of Colombia). Ocean & Coastal Management, 69: 133-142.

Ruessink, B. 1998. Bound and free infragravity waves in the nearshore zone under breaking and nonbreaking conditions. Journal of Geophysical Research, 103: 12795-12805. doi: 10.1029/98JC00893

Ruiz-Merchán, J., Otero, L., Conde, M., et al. 2019. Field observations of wave and current characteristics on a microtidal reflective beach. Journal of Coastal Research, 35: 1164-1184.

Ruiz-Merchán, J., Restrepo, J., Haus, B.K., et al. 2025. Field observations of wave and current dynamics on a microtidal dissipative-intermediate beach at Bocagrande, Colombian Caribbean during dry and wet seasons. Latin American Journal of Aquatic Research, 53: 801-822. doi: 10.3856/vol53-issue5-fulltext-3481

Russell, P. 1993. Mechanisms for beach erosion during storms. Continental Shelf Research, 13: 1243-1265.

Sahin, C., Verney, R., Sheremet, A., et al. 2017. Acoustic backscatter by suspended cohesive sediments: Field observations, Seine Estuary, France. Continental Shelf Research, 134: 39-51.

Sassi, M., Hoitink, A. & Vermeulen, B. 2012. Impact of sound attenuation by suspended sediment on ADCP backscatter calibrations. Water Resources Research, 48: 2012WR012008. doi: 10.1029/2012WR012008

Schaffer, H.A. 1994. Edge waves forced by short-wave groups. Journal of Fluid Mechanics, 259: S002211 2094000066. doi: 10.1017/S0022112094000066.

Scott, T., Masselink, G. & Russell, P. 2011. Morphodynamic characteristics and classification of beaches in England and Wales. Marine Geology, 286: 1-20. doi: 10.1016/j.margeo.2011.04.004

Short, F. & Neckles, H. 1999. The effects of global climate change on seagrasses. Aquatic Botany, 63: 169-196. doi: 10.1016/S0304-3770(98)00117-X

Symonds, G., Huntley, D. & Bowen, A. 1982. Two-dimensional surf beat: Long wave generation by a time-varying breakpoint. Journal of Geophysical Research, 87: 492-498. doi: 10.1029/JC087iC01p00492

Wiedemann, H. 1973. Reconnaissance of the Ciénaga Grande de Santa Marta, Colombia: physical parameters and geological history. Boletín de Investigaciones Marinas y Costeras, 7: 85-119.

Winter, G., Lowe, R., Symonds, G., et al. 2017. Standing infragravity waves over an alongshore irregular rocky bathymetry. Journal of Geophysical Research: Oceans, 122: 4868-4885. doi: 10.1002/2016JC012242

Wright, L. & Short, A. 1984. Morphodynamic variability of surf zones and beaches: a synthesis. Marine Geology, 56: 93-118.

Received: September 22, 2025; Accepted: March 3, 2026